Biosensors and Bioelectronics 126 (2019) 160–169

Contents lists available at ScienceDirect

Biosensors and Bioelectronics

journal homepage: www.elsevier.com/locate/bios

An ultrasensitive photoelectrochemical biosensor for glucose based on bio-derived nitrogen-doped carbon sheets wrapped titanium dioxide nanoparticles

Raji Atchudan[a,*,1], Nallal Muthuchamy[b,1], Thomas Nesakumar Jebakumar Immanuel Edison[a], Suguna Perumal[c], Rajangam Vinodh[d,1], Kang Hyun Park[b], Yong Rok Lee[a,*]

[a] School of Chemical Engineering, Yeungnam University, Gyeongsan 38541, Republic of Korea
[b] Department of Chemistry, Pusan National University, Busan 46241, Republic of Korea
[c] Department of Applied Chemistry, Kyungpook National University, Daegu 41566, Republic of Korea
[d] Department of Chemical Engineering, Hanseo University, Seosan 360-706, Republic of Korea

ARTICLE INFO

Keywords:
Photoelectrochemistry
Glucose biosensor
Titanium dioxide
Hydrothermal
Sol-gel
Peach fruit

ABSTRACT

In this work, an ultra-sensing photoelectrochemical (PEC) glucose biosensor has been constructed from the bio-derived nitrogen-doped carbon sheets (NDC) wrapped titanium dioxide nanoparticles (NDC-TiO_2 NPs) followed by the covalent immobilization of glucose oxidase (GODx) on them (designated as a GODx/NDC-TiO_2NPs/ITO biosensor). Initially, the TiO_2 NPs was synthesized by sol-gel method and then NDC-TiO_2 NPs was synthesized utilizing a green source of *Prunus persica* (peach fruit) through a simple hydrothermal process. The synthesized NDC-TiO_2 NPs composite was characterized by FESEM, HRTEM, Raman spectroscopy, XRD, ATR-FTIR spectroscopy and XPS to determine composition and phase purity. These fabricated GODx/NDC-TiO_2NPs/ITO biosensor exhibited a good charge separation, highly enhanced and stable photocurrent responses with switching PEC behavior under the light ($\lambda > 400$ nm). As a result, GODx/NDC-TiO_2NPs/ITO PEC glucose sensor exhibits a good photocurrent response to detection of glucose concentrations (0.05–10 μM) with an ultra-low detection limit of 13 nM under optimized PEC experimental conditions. Also, the PEC glucose sensor revealed a high selectivity, good stability, long time durability, and capability to analyze the glucose levels in real human serum. Also, the further development of this work may provide new insights into preparing other bio-derived carbon nanostructure-based photocatalysts for PEC applications.

1. Introduction

Recently, photoelectrochemical (PEC) biosensing have gained considerable attention among the other biosensing methods due to their promising performances such as high sensitivity, negligible background current and the clear separation of the detection signals from the excitation source (Zhao et al., 2014; Devadoss et al., 2015). The PEC measurement is an intensely developing technique and this possesses the wide advantages on highly sensitive biosensors due to the low background current responses from the combination of electrochemical and coupling light excitation. Moreover, compared with all-optical detection methods, such as fluorescence, expensive optical imaging devices and require complex and sophisticated image recognition software, the cost-effective electrochemical instrumentation makes the PEC method is a rapid, simple and economical for successful biosensor applications (Bettazzi et al., 2018; Nallal et al., 2017). Considerable research interest in PEC biosensor is increasing in the detection of various specific targets in bio-system such as antigens, enzymes, enzyme substrates, nucleic acids, proteins and chemicals due to the rise of novel photo-electrochemically active species and detection schemes (Ibrahim et al., 2018). The characteristic of PEC biosensing interface is generally composed of photo-electroactive materials and biological receptors. Photo-electroactive materials served as the energy transducer layer to generate photocurrents ($j_{(photo)}$) upon illumination. Besides, this transducer layer offers suitable supports for immobilization of biological receptors and these receptors can selectively recognize and capture target analytes. Therefore, the fabrication of the transducer layer has been of great importance for the PEC applications. Recently,

* Corresponding authors.
E-mail addresses: atchudanr@yu.ac.kr (R. Atchudan), yrlee@yu.ac.kr (Y.R. Lee).
[1] Authors contributed equally to this work.

https://doi.org/10.1016/j.bios.2018.10.049
Received 27 August 2018; Received in revised form 12 October 2018; Accepted 23 October 2018
Available online 26 October 2018
0956-5663/

the photo-electroactive nanomaterials have been considered as an ultimate choice for the fabrication of the PEC sensing interface (Muthuchamy et al., 2017; Gopalan et al., 2017). In general, various semiconducting nanoparticles have been widely used in the PEC sensor and which showed superior sensing performance due to their efficient multiple charge-carrier generations and size-tunable optical and electronic properties, particularly, the semiconducting nanostructures play a significant role in PEC biosensors due to its good electrical and optical properties, superior physicochemical stability, earth-abundance, and cost efficiency. However, the PEC efficiency of pristine semiconductors is still limited due to the high recombination rate of photogenerated electron-hole pairs (e^- and h^+), the relative optical band gap and grain boundaries (Zhao et al., 2018; Dai et al., 2015).

On the other hand, the traditional nanomaterial (*e.g.* polymer hydrogels; functionalized conducting polymers) based biosensors with high porosity will provide a high loading of nanoparticles without major aggregation and these materials enable the electrolytes in the host-guest interface. However, those polymer hydrogels show the poor conductivity in electrochemistry. This drawback was overcome by the highly conductive carbon nanostructured materials (*e.g.* graphene (Gr) and carbon nanotubes (CNT)) due to their remarkable large surface area even after tightly packing of various guest nanomaterials on the surface of the host framework (Gopalan et al., 2018; Hao et al., 2017; Komathi et al., 2016). Moreover, the introduction of heteroatoms such as nitrogen into the framework of Gr and its derived nanomaterials can significantly improve the conductivity and enhance the PEC performance (Chen et al., 2013). But generally, the preparation of Gr is done using an expensive process and results in the expulsion of toxic waste during their synthesis. Hence, scientist trusts the bio-derived Gr-like carbon sheets as a host material to hold the guest species of the active nanoparticles suitable for PEC biosensor. The bio-derived Gr-like carbon sheets are eco-friendly as well as various functional groups including nitrogen-containing components present on their surface enhance the electrochemical properties towards PEC biosensor and so on (Santhiago et al., 2018; Atchudan et al., 2018a). To the best of our knowledge, bio-derived nitrogen-doped carbon sheets wrapped titanium dioxide nanoparticles has not been utilized in PEC biosensor research until now. Herein, a novel and ultrasensitive nitrogen-doped carbon sheets (NDC) wrapped titanium dioxide nanoparticles (NDC-TiO_2 NPs) nanocomposite was prepared *via* the simple hydrothermal method. Also, the strong interactions between TiO_2 NPs and the NDC sheet were confirmed by various physicochemical techniques including X-ray photoelectron spectroscopy (XPS), Attenuated total reflectance Fourier transform infrared spectroscopy (ATR-FTIR) and High-resolution transmission electron microscopy (HRTEM).

Glucose (Glu) is a major source of energy for cell metabolism and regulation, also it has a main role in the process of natural cell growth. Moreover, if Glu level is an excess or deficiency in a body might effect on cell functions. A few recent studies focused to determine the high concentration of Glu in diagnosing system. However, on the other hand, still existing a big challenge to monitor the accuracy level of Glu, most importantly in the low-level Glu detection due to lack of improvements in sensor fabrication (Vashist, 2012). To overcome this ultra-low detection of Glu, herein, PEC Glu biosensor has been developed by the functionalization of glucose oxidase (GODx) on the surface of NDC-TiO_2 NPs coated indium tin oxide (ITO) electrode (designated as a GODx/NDC-TiO_2NPs/ITO biosensor). The plausible mechanism was systematically investigated to find the enhancement of PEC as a Glu biosensor under the light. This proposed PEC biosensor exhibited good PEC performances towards ultradetection of Glu biomolecules with a low detection range of 13 nM and a wide linear range (0.05–10 μM). In addition, fabricated GODx/NDC-TiO_2NPs/ITO biosensor was utilized for determination of Glu levels in real human blood serum system. Overall, the PEC result indicated that the GODx/NDC-TiO_2NPs/ITO biosensor is a promising material for developing high-performance PEC biosensor for the biomedical, health care, food industry, and environmental analysis.

2. Experimental

2.1. Materials

The peach fruit was collected from the Kyungpook National University Campus, Daegu, Republic of Korea. Titanium (IV) isopropoxide, anhydrous ethanol, aqueous ammonia, 3-aminopropyltriethoxysilane (3-APTES), glucose, glutaraldehyde, human serum (from human male AB plasma, USA origin, sterile-filtered), 5% Nafion, GODx (from Aspergillus niger; E.C 1.1.3.4, 151 U mg^{-1}, U: enzyme units); phosphate buffer solutions (PBS) and sulfuric acid were purchased from Sigma-Aldrich and were used as received. The double distilled (DD) water was used throughout this study.

2.2. Synthesis of the bare TiO_2 NPs and NDC-TiO_2 NPs

The bare TiO_2 NPs were synthesized by a simple sol-gel method as per our previously reported work (Atchudan et al., 2017). The NDC-TiO_2 NPs was synthesized through a hydrothermal method. Typically, 30 mL of peach juice, 200 mg of TiO_2 NPs and 1 mL of aqueous ammonia were taken into a Teflon-lined stainless steel autoclave. The mixture was subsequently heated at 180 °C for 12 h and then cooled to room temperature. The resultant mixture was filtered and washed with DD water. The residue was dried at 70 °C for 12 h. The obtained brownish-black powder denoted as NDC-TiO_2 NPs. Schematic illustration of the synthesis procedure is clearly seen in Fig. S1.

2.3. Fabrication of GODx/NDC-TiO_2NPs/ITO biosensor

Prior to the fabrication of NDC-TiO_2NPs/ITO biosensor, the indium tin oxide (ITO) substrates were pre-treated by ultrasonication process in ethanol, acetone and followed by distilled water. Subsequently, dried under nitrogen (N_2) stream. Initially, about 5 mg of NDC-TiO_2NPs were dispersed in about 3:3:1 (v/v) in distilled water, isopropyl alcohol and Nafion (5% in ethanol) under the ultrasonication for 1 h. About 6 μL of the above-dispersed slurry was drop-cast on the surface of a pre-treated ITO electrode (area = 0.25 cm^2 and catalyst loading = 171.5 μg cm^{-2}) and dried in air. After that, NDC-TiO_2NPs/ITO electrode silanized using 3-APTES. NDC-TiO_2NPs/ITO electrode was incubated in a solution containing 3-APTES (1 mL), 5% anhydrous ethanol (5 mL), 28% ammonia (0.25 mL) and dried in an oven at 120 °C for 1 h. Further, the silanized NDC-TiO_2NPs/ITO electrode was incubated with glutaraldehyde solution at 37 °C for 2 h to link the aldehyde groups on the NDC-TiO_2NPs/ITO surface (*via* glutaraldehyde/silane linkage chemistry). Finally, the NDC-TiO_2NPs/ITO electrode was incubated with GODx (1 mg mL^{-1} in 0.1 M PBS at pH 7) at 4 °C for 24 h and designated as a GODx/NDC-TiO_2NPs/ITO biosensor. For the long period stability and durability analysis, the fabricated NDC-TiO_2NPs/ITO biosensor was stored in 0.1 M PBS at pH 7 and 4 °C for use.

2.4. PEC glucose measurements

PEC measurements were performed using CHI 760D potentiostat CH instrument. An aqueous solution of 0.1 M PBS (pH 7) was used as the electrolyte. The NDC-TiO_2NPs coated ITO surface area was exposed to the electrolyte and then soaked in the aqueous 0.1 M PBS (pH 7). Also, the uncoated ITO electrode surface area was sealed using epoxy for insulation. The light was illuminated on the front side of the NDC-TiO_2NPs/ITO biosensor using a conventional three-electrode set-up, NDC-TiO_2NPs/ITO biosensor (working electrode), $Ag/AgCl_{(sat.\ KCl)}$ (reference electrode), and platinum wire (counter electrode) in an analyst solution through a quartz window. Both, cyclic voltammetry (CV) and

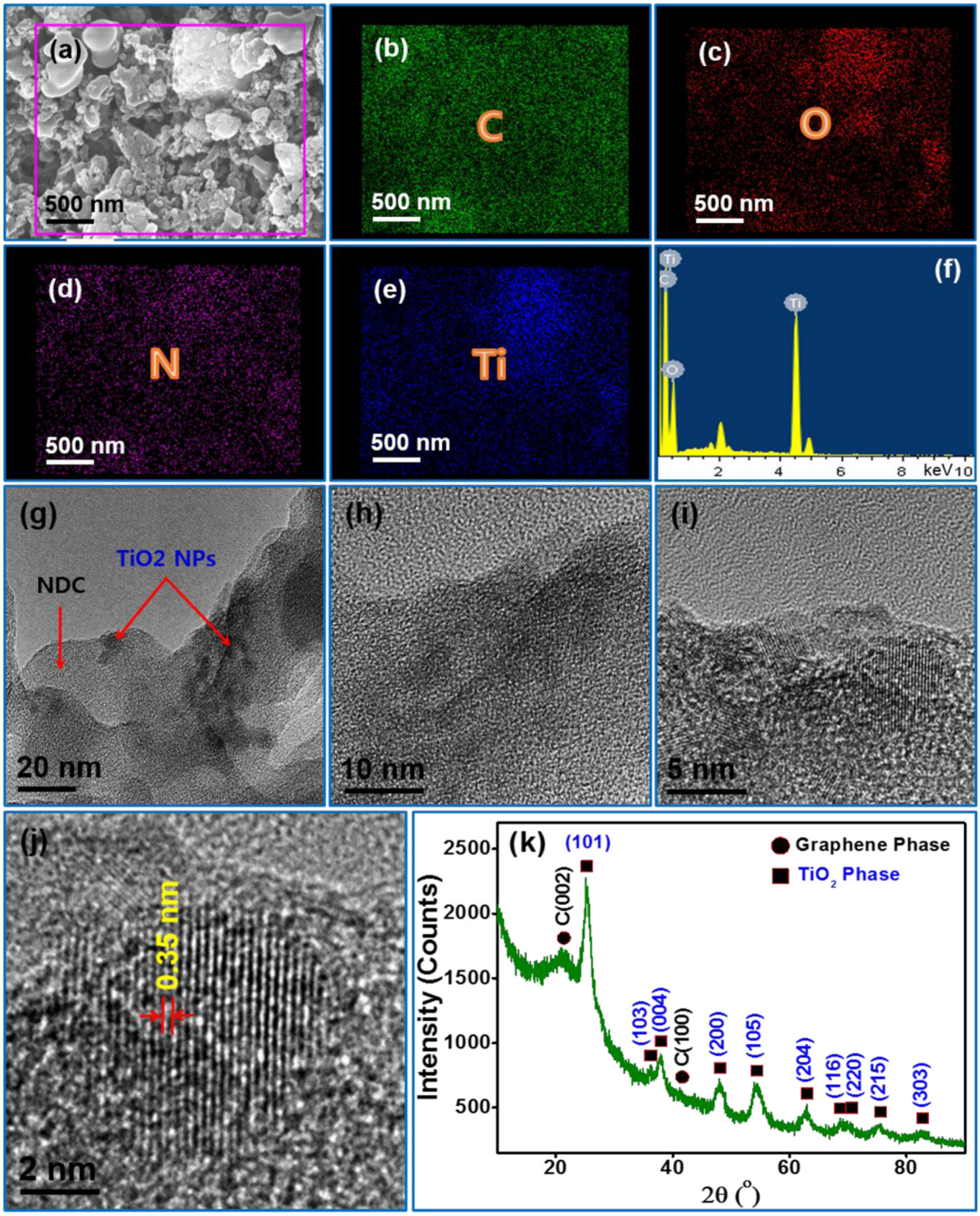

Fig. 1. (a) FESEM image, and the corresponding elemental mapping of (b) carbon, (c) oxygen, (d) nitrogen, (e) Titanium and (f) EDX spectrum of the synthesized NDC-TiO_2 NPs. (g)-(j) HRTEM images with different magnification and (k) XRD pattern of the synthesized NDC-TiO_2 NPs.

linear sweep voltammetry (LSV) measurements were performed at a scan rate of 20 mV s^{-1}. The electrochemical impedance spectroscopy (EIS, Nyquist plots) was recorded in an AC potential range between 100 kHz and 10 Hz with an amplitude of 10 mV. The photo-chronoamperomatric measurements were performed on the constant applied potential of 0.40 V. A 300 W xenon lamp system (model 66184, Oriel Instrument) with an optical filter ($\lambda > 400$ nm) was used as a light source and installed 10 cm away from the PEC cell.

3. Results and discussion

3.1. Characterization of the synthesized bare TiO_2 NPs and NDC-TiO_2 NPs

FESEM was used to observe the surface morphology of the synthesized materials. Fig. S2 shows the FESEM images with energy-dispersive X-ray (EDX) spectrum of the synthesized bare TiO_2 NPs. The aggregated nanoparticles are vividly seen in Fig. S2(a-d). Further, the elemental

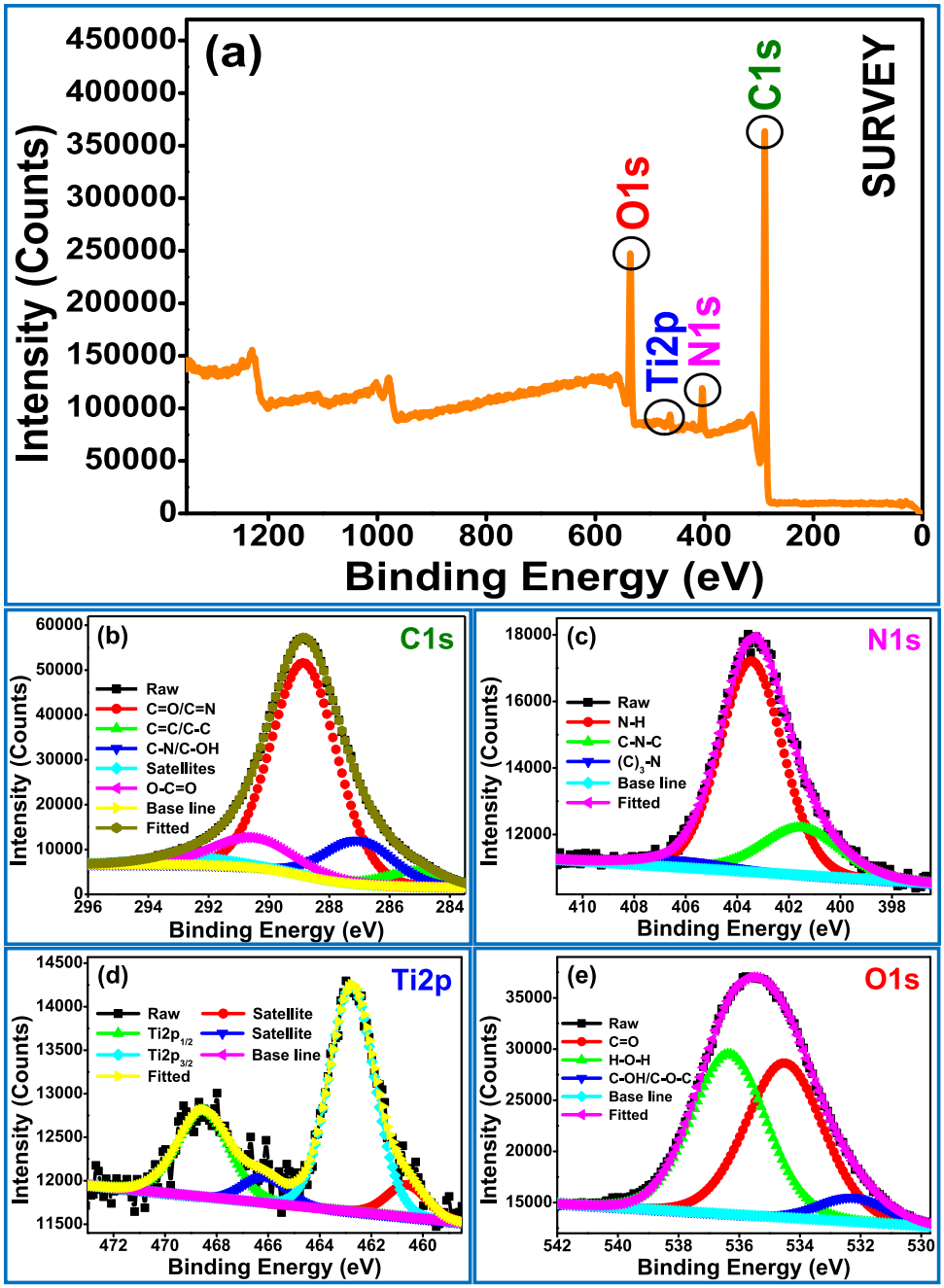

Fig. 2. (a) XPS survey scan spectrum and high-resolution spectra of (b) C 1s, (c) N 1s, (d) Ti 2p and (e) O 1s for the synthesized NDC-TiO_2 NPs.

compositions (Ti and O) of TiO_2 NPs was confirmed by EDX spectrum (Fig. S2(e)). The peak above 2 keV corresponds to the Si which is originated from the si-wafer. Beyond this absence of impurities are observed in the spectrum which supports the high purity of the synthesized TiO_2 NPs. As shown in Fig. 1(a), the synthesized NDC-TiO_2 NPs presented nanoparticles embedded in the carbon sheets. The composition of elements was confirmed by the EDX mapping analysis. It can be seen that the elements such as C, O, N and Ti are uniformly distributed in the composite (Fig. 1(b-e)). This result provides evidence for the presence of Ti on the surface of the N-doped carbon sheets. Further, the elemental composition also evident by EDX spectral analysis (Fig. 1(f)). The morphology of the synthesized NDC-TiO_2 NPs was further investigated by HRTEM. As shown in Fig. 1(g-j), the TiO_2 NPs are (dark particles, Fig. 1(g)) distributed on the N-doped carbon sheets. The densely bound TiO_2 NPs are around 5 ± 2 nm with high crystalline in nature. The lattice fringes are clearly seen with a lattice spacing of about 0.35 nm which is related to the (101) plane of anatase TiO_2 (Fig. 1(j)).

XRD is one of the most common techniques used to study the properties of the materials. Fig. 1(k) shows the diffraction pattern of the synthesized NDC-TiO_2 NPs, all the characteristic signals of TiO_2 were observed at the 2θ of 25.1, 36.2, 37.9, 47.9, 54.1, 62.9, 68.6, 70.3, 75.5, and 82.6° can be ascribed to the (101), (103), (004), (200), (105), (204), (116), (220), (215) and (303) planes of anatase structure TiO_2, respectively which is in good accordance with the JCPDS No. 84-1285 (Gnanasekaran et al., 2015; Atchudan et al., 2018b). In addition, the peak appeared around 21.7 and 41.5° corresponds to the (002) and (100) plane of hexagonal graphene-like carbon structure. The peak position of the (002) plane is observed at lower 2θ value when compared to standard Gr structure due to the functional group (N) within

the graphitic carbon framework and also partial graphitization of the carbon structure. The absence of impurities peaks confirms the purity of the synthesized NDC-TiO_2 NPs. The average size of the TiO_2 NPs was 5 nm with the lattice spacing of 0.35 nm within the synthesized NDC-TiO_2 NPs according to the (101) reflection and these results resemble with the HRTEM result. To further verify the formation of NDC-TiO_2 NPs, the composite was characterized by Raman spectroscopy. The Raman spectrum of the NDC-TiO_2 NPs is shown in Fig. S3. The D and G-band can be found at 1370 and 1597 cm^{-1}, respectively. The synthesized NDC-TiO_2 NPs have an I_D/I_G ratio of *ca.* 0.65, and the low intensity of the D-band associated with the minor defects in the sp^2 carbon lattice indicated the doping of N into the carbon framework (Li et al., 2013; Lou et al., 2013). The bands observed at lower wavenumber region (below 1000 cm^{-1}) correspond to the anatase TiO_2 phases. Thus, the results suggest the anatase phases of TiO_2 NPs are presented on the moderate Gr-based carbon sheets surface.

ATR-FTIR spectroscopy is one of the most suitable measurements used to identify the chemical composition and structure of the resulting materials. Fig. S4 represents the ATR-FTIR spectrum of the synthesized NDC-TiO_2 NPs, the broad absorption peak around 3250 cm^{-1} belongs to the stretching vibration of –OH groups, which are related to the bonded hydroxyl/carboxyl OH, bound water and free water that may absorb on the surface of the NDC. The absorption band at 2926 and 2857 cm^{-1} is attributed to the vibration of C−H asymmetric and symmetric stretching vibrations, respectively. The characteristic absorption bands of C=O, C=C, C−N, and C−OH stretching vibrations at 1709, 1612, 1441 and 1371 cm^{-1}, respectively (Ding et al., 2014; Campos et al., 2015). Inset of Fig. S4 clearly displays the C=O stretching vibrations of the NDC-TiO_2 NPs. The absorption band between the 1280 and 1017 cm^{-1} are ascribed to the presence of C−O−C stretching vibrations in the NDC (Li et al., 2015). The presence C−N stretching vibration band as well as absence of N–H stretching vibration band confirms the N-atom chemically bonded with carbon (NDS) framework. Apart from these vibration bands, the sharp intense band around 578 cm^{-1} represents the framework vibrations of Ti−O bonds. Moreover, the absence of Ti-C or Ti−O−C bonds suggesting that the TiO_2 NPs are physically anchored with the NDC (There is no chemical bond between the NDC and TiO_2 NPs). The FTIR results concluding the TiO_2 NPs are attached over the hydroxyl and carboxyl functionalized NDC without any contamination. The chemical composition and electronic state of the resulting NDC-TiO_2 NPs were revealed by XPS. As shown in Fig. 2(a), the survey spectrum of synthesized NDC-TiO_2 NPs exhibits four obvious peaks can be ascribed to C1s, O1s, N1s, and Ti2p. The C1s binding energy peak can be deconvoluted into four characteristic peaks C=C/C−C, C−N/C−OH, C=O/C=N and O−C=O at the position of 284.98, 286.58, 288.68 and 290.68 eV, respectively which is shown in Fig. 2(b) (Zhang and Chen, 2014; Niu et al., 2015; Yang et al., 2014). The satellite peaks occur at 292.28 eV contributes to the carbon-containing functional groups. The deconvoluted spectrum of N1s binding energy peak (Fig. 2(c)) showed three predominant peaks with a binding energy of 401.58, 403.48 and 406.28 eV attributed to C−N–C, N–H and $(C)_3$–N groups, respectively (Ju and Chen, 2014). The high-resolution spectrum of the Ti2p binding energy region (Fig. 2(d)) can be fitted to two major peaks at 462.78 and 468.58 eV which is attributed to $Ti2p_{3/2}$ and $Ti2p_{1/2}$, respectively. The high-resolution O1s spectrum (Fig. 2(e)) shows three peaks at 532.38, 534.48 and 536.38 eV, which corresponds to the C−OH/C−O−C, C=O and H−O−H groups, respectively (Atchudan et al., 2018c). These results suggest that the synthesized NDC-TiO_2 NPs consists of C, O, N, and Ti with high purity.

3.2. Photoelectrochemical properties of GODx/NDC-TiO_2NPs/ITO biosensor

The fabricated GODx/NDC-TiO_2NPs/ITO biosensor was characterized by the EIS measurements, which is a powerful tool for probing the charge transfer resistance (R_{ct}) and separation efficiency between the photogenerated e^- and h^+ of the GODx/NDC-TiO_2NPs/ITO biosensor. Nyquist plot spectra of GODx/NDC-TiO_2NPs/ITO biosensor with representative semicircles are provided in Fig. 3(A) for both light OFF and ON conditions. The semicircle radius in the EIS Nyquist plot resembles the R_{ct} of the fabricated biosensor. GODx/NDC-TiO_2NPs/ITO biosensor under light ON condition shows a small semicircle radius at a higher frequency range represents the highest charge transfer efficiency and low R_{ct} than light OFF at the surface of the electrode. The lower real (Z_{re}) and imaginary (Z_{im}) resistant of GODx/NDC-TiO_2NPs/ITO biosensor (under light ON) suggest that it provided a good interface for charge transfer. The active surface area (A) of NDC-TiO_2NPs/ITO electrode was calculated by using the Randles−Sevcik equation (Fig. S5). From the slope of the plot of I_p *vs.* $\nu^{1/2}$, A of the NDC-TiO_2NPs/ITO electrode was found to be 0.6768 cm^2. The synergistic contribution of light on the PEC responses towards Glu on the GODx/NDC-TiO_2NPs/ITO biosensor was investigated by CV (Fig. 3B), LSV (Fig. 3C) and CA (Fig. 3D) techniques in the absence and presence 2 μM of Glu in 0.1 M PBS (pH 7.0). In the absence of Glu, the GODx/NDC-TiO_2NPs/ITO biosensor exhibited negligible background current response in light OFF (Fig. 3B(a)). Upon light ON condition (Fig. 3B(b)), overall current response slightly enhanced linearly with applied potentials due to the high efficient photoabsorption and charge carrier separation by the GODx/NDC-TiO_2NPs/ITO biosensor. After adding 2 μM of Glu into the electrolytic solution, GODx/NDC-TiO_2NPs/ITO biosensor exhibited an increased trend of anodic peak current around 0.20–0.60 V *vs.* Ag/AgCl (Fig. 3B(c)) at light OFF condition. At the same condition, the anodic peak current (Fig. 3B(d)) remarkably increased almost two times in light ON. This also confirmed by the $j_{(photo)}$ *versus V* ($j_{(photo)}$-*V*) (Fig. 3C) and $j_{(photo)}$ *versus t* ($j_{(photo)}$-*t*) (Fig. 3D) plots. The $j_{(photo)}$-*V* measured in absence of Glu, GODx/NDC-TiO_2NPs/ITO (Fig. 3C(b)) shows ~ 22.6-time high $j_{(photo)}$ value compared with under dark condition response Fig. 3(C)(a). However, in the presence of 2 μM of Glu concentration ([Glu]), GODx/NDC-TiO_2NPs/ITO biosensor shows an oxidation peak at bias potential + 0.40 V *vs.* Ag/AgCl for both conditions such as light OFF (Fig. 3C(c)) and light ON (Fig. 3C(d)). Notably, the maximum $j_{(photo)}$ was obtained for GODx/NDC-TiO_2NPs/ITO biosensor when the light was in ON condition (Fig. 3C(d)) (~3.55 times higher than that of light OFF condition (Fig. 3C(c)), which confirms that fabricated GODx/NDC-TiO_2NPs/ITO have good advantageous for both low background and energy saving towards PEC Glu detection. The $j_{(photo)}$-t plot under the light ON (Fig. 3D(a′)) shows a stable background $j_{(photo)}$ at 0.4 V *vs.* Ag/AgCl resulting from the PEC water oxidation at the surface of GODx/NDC-TiO_2NPs/ITO. Moreover, from the Fig. 3(D)(a) it is clear that ~2 times higher $j_{(photo)}$ value with the addition of Glu (2 μM), this confirms that our PEC Glu biosensor is attributed to the PEC generated charge carriers. At the same applied potential 0.4 V *vs.* Ag/AgCl, when the light was OFF the GODx/NDC-TiO_2NPs/ITO biosensor shows ~ 3.5 time lower *j* value (Fig. S6), due to the normal electrocatalytic Glu oxidation. For the comparison and to find out the role of individual components in fabricating biosensor, PEC experiments were also performed for GODx/TiO_2NPs/ITO (Fig. 3D(b and b′)) and GODx/NDC/ITO (Fig. 3D(c and c′)) in both presence and absence of [2 μM] Glu under light ON. The PEC result shows that the values of $j_{(photo)}$ in the following order: GODx/NDC-TiO_2NPs/ITO > GODx/TiO_2NPs/ITO > GODx/NDC/ITO (Fig. 3D). Whereas, the GODx/NDC-TiO_2NPs/ITO biosensor showed a $j_{(photo)}$ of 0.96 μA cm^{-2} for 2 μM [Glu], which is 15 and 7 times higher than GODx/TiO_2NPs/ITO and GODx/NDC/ITO, respectively. These results clearly indicate the better improvement of the $j_{(photo)}$ conversion efficiency of TiO_2 NPs in the presence of bio-derived NDC because of the highly conducting nature and strong e^- coupling between the excited-state NDC and conduction band (CB) of TiO_2 NPs. Additionally, in Fig. 3(C)(b) and Fig. 3(D)(a′), GODx/NDC-TiO_2NPs/ITO shows high $j_{(photo)}$ response were observed over the oxygen evolution reaction (OER) potential range with the onset potential (E_{onset}) of 0.63 V *vs.* Ag/AgCl (Fig. 3C (b)), which is interesting that our GODx/NDC-TiO_2NPs/ITO is a potential photocatalyst for PEC

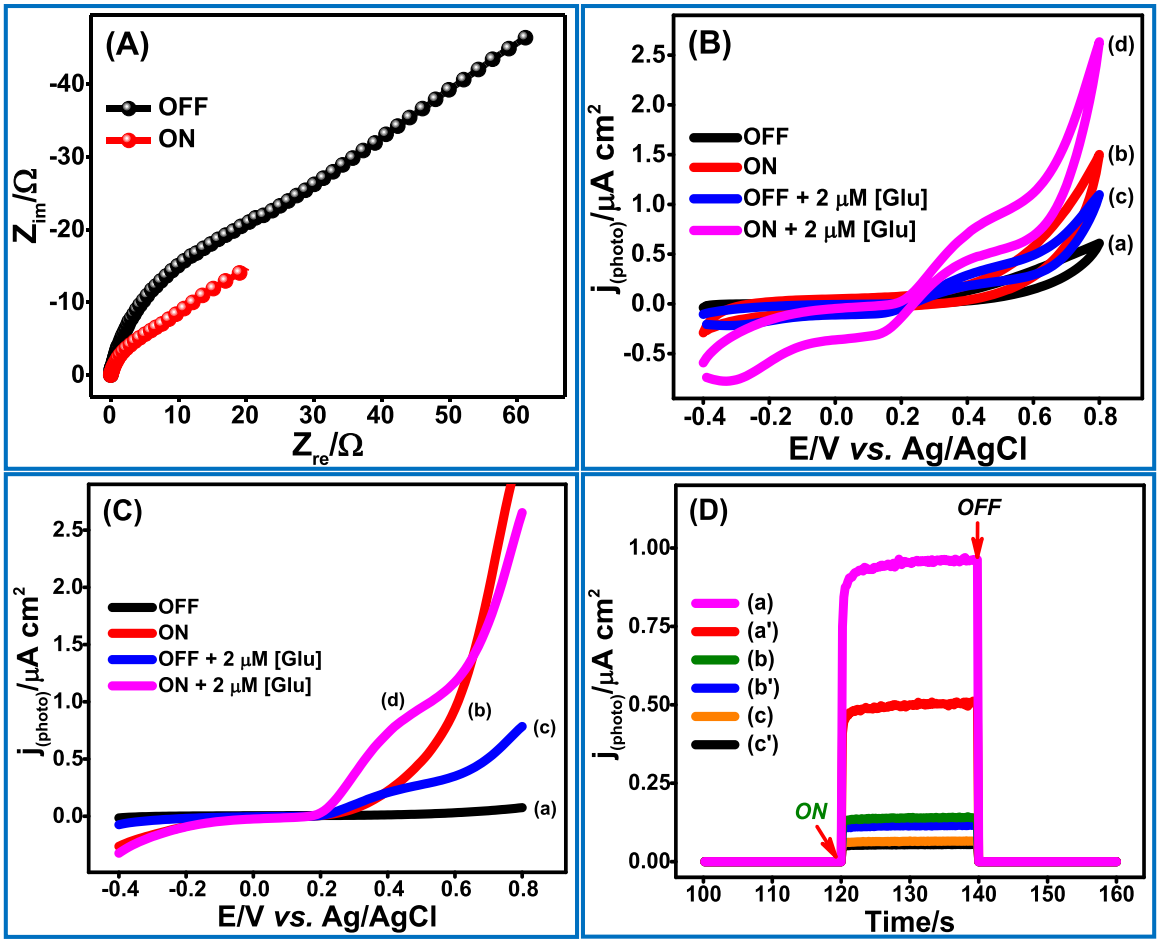

Fig. 3. (A) Electrochemical impedance spectroscopy (Nyquist plots); **(B)** Cyclic voltammograms and **(C)** Linear sweep voltammograms were obtained at GODx/NDC-TiO_2NPs/ITO electrode in the (a, b) absence and (c, d) presence of 2 μM of glucose with (a,c) light OFF and (b, d) ON. **(D)** The $j_{(photo)}$-t responses of GODx/NDC-TiO_2NPs/ITO (a, a′); GODx/TiO_2NPs/ITO (b, b′) and GODx/NDC/ITO (c, c′) electrodes in the presence (a, b, c) and absence (a′, b′, c′) of 2 μM of Glu in 0.1 M pH 7.0 PBS at 0.40 V *vs.* Ag/AgCl.

water splitting application. Also, we were noticing that the GODx/NDC-TiO_2NPs/ITO electrode takes very few seconds of rising time to reach the stable $j_{(photo)}$ (Fig. 3D(a) and (a′)). Finally, these observations, such as low R_{ct}, high charge transfer efficiency, high A value, less rising time, low bias potential and stable as well as high $j_{(photo)}$ towards PEC Glu sensor confirming the successful fabrication of GODx/NDC-TiO_2NPs/ITO biosensor.

3.3. PEC experimental conditions optimization

To generate a high $j_{(photo)}$ response on the PEC Glu biosensor, the variable experimental conditions such as the effect of catalyst loading, GODx loading, supporting electrolyte pH value and applied potential on $j_{(photo)}$ were optimized and as shown in Fig. S7-S10. Initially, the loading effect of NDC-TiO_2NPs on the surface of the ITO electrode was investigated, and the optimized maximum $j_{(photo)}$ was obtained on the catalyst weight loading of 171.5 μg cm^{-2} (Fig. S7). Also, the GODx loading on the surface of NDC-TiO_2NPs/ITO was investigated by varying the concentration of GODx in an inhibition solution. The maximum $j_{(photo)}$ was obtained when the NDC-TiO_2NPs/ITO electrode was incubated with 1 mg mL^{-1} concentration of GODx in 0.1 M PBS at pH 7 (Fig. S8). Additionally, to confirming the suitable pH value, the PEC experiments were carried out under various pH ranges of supporting electrolyte. Fig. S9 shows that the $j_{(photo)}$ value increase with pH from pH 2.0 and reached its highest at pH 7.0. Beyond pH 7.0, the $j_{(photo)}$ value shows the decreasing trend. It might be of the immobilized GODx loses its bioactivity similar like results on already reported for GODx immobilized Glu sensors (Muthuchamy et al., 2018; Komathi et al., 2017). Finally, considering the importance of applied potential relevant to the $j_{(photo)}$ in GODx/NDC-TiO_2NPs/ITO biosensor is thus optimized. Fig. S10 illustrates that the $j_{(photo)}$ increase with applied potential between + 0.20 – + 0.40 V *vs.* Ag/AgCl, and then $j_{(photo)}$ decreases gradually with increase in applied potential (higher than +0.40 V *vs.* Ag/AgCl in 0.1 M PBS (pH 7.0)) containing 2 μM of Glu. Thus, an optimized condition such as catalyst loading = 171.5 μg cm^{-2}, GODx = 1 mg mL^{-1}, pH = 7 and applied potential + 0.40 V *vs.* Ag/AgCl were used in the PEC Glu biosensor experiments.

3.4. PEC mechanism and analytical performance of GODx/NDC-TiO_2NPs/ITO biosensor for glucose

We proposed the plausible mechanism for the PEC Glu detection on GODx/NDC-TiO_2NPs/ITO biosensor under light ON. In Fig. 4(A), the Schematic diagram illustrates that the energy level of the valence band (VB) and CB of NDC are at a higher level than those TiO_2 NPs, which is useful for the migration of generated e^- and $h^+$of PEC and minimize their recombination. The FAD redox group in GODx oxidizes Glu analyte to gluconic acid and simultaneously reduced to $FADH_2$ with close attachment and enhanced shifting of PEC, generate h^+. The results in Fig. S8 also confirming that the $j_{(photo)}$ of GODx/NDC-TiO_2NPs/ITO (at 1 mg mL^{-1} concentration of GODx) is ~5.5 times higher than that of without GODx in 2 μM of Glu. Under light ON, due to the very low

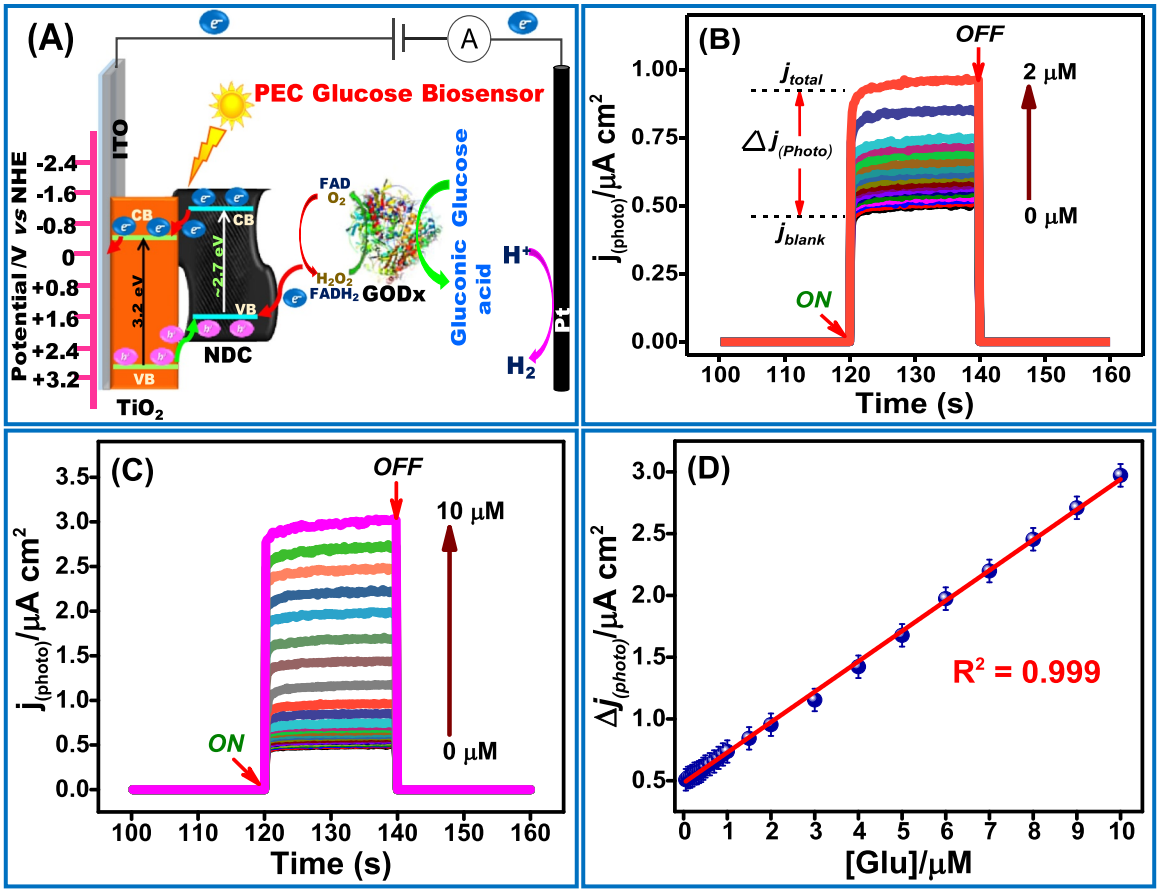

Fig. 4. (A) The schematic plausible mechanism for PEC Glu sensing at GODx/NDC-TiO_2NPs/ITO. **(B)** The $j_{(photo)}$-*t* responses of GODx/NDC-TiO_2NPs/ITO toward Glu at increasing concentration from 0 μM to 2 μM and **(C)** from 0 μM to 10 μM in the supporting electrolyte of 0.1 M pH 7.0. **(D)** Linear calibration ([Glu] *vs.* $j_{(photo)}$) curve. Error bars indicate the standard deviation of three repeated measurements.

Table 1
Comparison of the performances of PEC Glu biosensor based on GODx/NDC-TiO_2NPs/ITO with other reported Glu biosensors.

Materials	Analytical methods	Detection limit	Linear range	Sensitivity	Reference
BiOI/NiO/ITO	PEC	1.6 μM	0.005–10 mM	–	(Zhang et al., 2018)
a-MoSx/RGO/ ITO	PEC	0.098 mM	0.15–16 mM	–	(Shang et al., 2018)
TiO_2(G) NW@PAPBA- Au HJNH	PEC	0.11 mM	0.5–28 mM	549.58 μA mM^{-1} cm^{-2}	(Nallal et al., 2017)
Au/CuS/TiO_2	PEC	30 nM	0.1–3.0 μM	–	(Wang et al., 2018)
GOx|g-C_3N_4-TiO_2|ITO	PEC	0.01 mM	0.05–16 mM	16.7 μA mM^{-1} cm^{-2}	(Liu et al., 2017a)
ITO/MoS_2-TiO_2/GOx	PEC	0.015 mM	0.1–10 mM	0.81 μA mM^{-1}	(Liu et al., 2017b)
TiO_2–GR	Electrochemistry	–	0.0–8 mM	6.2 μA mM^{-1} cm^{-2}	(Jang et al., 2012)
GOD/HNF–TiO_2/GC	Electrochemistry	0.8 μM	0.002–3.17 mM	32.6 μA mM^{-1} cm^{-2}	(Guo et al., 2017)
GOx-GQDs	Electrochemistry	1.35 μM	10 μM–3 mM	0.00769 μA $μM^{-1}$ cm^{-2}	(Gupta et al., 2018)
Cu_2Se SPs/CF	Electrochemistry	0.25 μM	0.00025–0.237 mM	18,660 μA mM^{-1} cm^{-2}	(Zhu et al., 2018)
Ni@*f*-MWCNT/GCE	Electrochemistry	0.021 μM	0.05–12.0 mM	–	(Başkaya et al., 2017)
GODx/NDC-TiO_2NPs/ITO	PEC	13 nM	0.05–10 μM	215 nA $μM^{-1}$ cm^{-2}	This work

oxidation potential of H_2O_2, GODx on NDC-TiO_2NPs/ITO surface has capable of reduction of O_2 molecules to H_2O_2. Those H_2O_2 molecules can be acted as an efficient e^- donor for shifting of PEC generated h^+ on NDC and thus e^- transferred to conductive ITO, while the PEC generated h^+ in the VB (TiO_2 NPs), it migrates to the VB of NDC (Fig. 4A). Finally, the increased $j_{(photo)}$ was monitored due to the utilization of H_2O_2 by PEC. As a proof-of-concept, GODx/NDC-TiO_2NPs/ITO PEC biosensor exhibits a good $j_{(photo)}$ responses to the concentrations of Glu (Fig. 4B-D).

The $j_{(photo)}$-*t* curve of GODx/NDC-TiO_2NPs/ITO biosensor clearly demonstrates the fast PEC responses of the fabricated biosensor to Glu under optimal conditions. As seen in Fig. 4B and C, under the light ON, without Glu shows a stable background photocurrent (j_{blank}) due to the PEC water oxidation reaction at the GODx/NDC-TiO_2NPs/ITO biosensor surface. Also, the PEC responses (j_{total}) increase with each addition of [Glu] (ranges from 50 nM to 2 μM in Fig. 4B and from 50 nM to 10 μM in Fig. 4C). These increase [Glu] directs to an increase in the PEC responses of the j_{total}, suggesting a good correlation of the PEC ultra-detection rate of the of GODx/NDC-TiO_2NPs/ITO biosensor with the different [Glu] in 0.1 M PBS (pH 7.0). This same PEC Glu detection experiments repeated three times, and the j_{total} have featured highly reproducible PEC Glu sensing responses. From the PEC responses with diverse [Glu], a net steady-state ($\Delta j_{(photo)}$) can be calculated by subtraction j_{blank} from j_{total} (Eq. (1)). Also, the calculated $\Delta j_{(photo)}$ values change with different [Glu] are summarized and plotted in the corresponding [Glu] *versus* $\Delta j_{(photo)}$) calibration curve in Fig. 4(D).

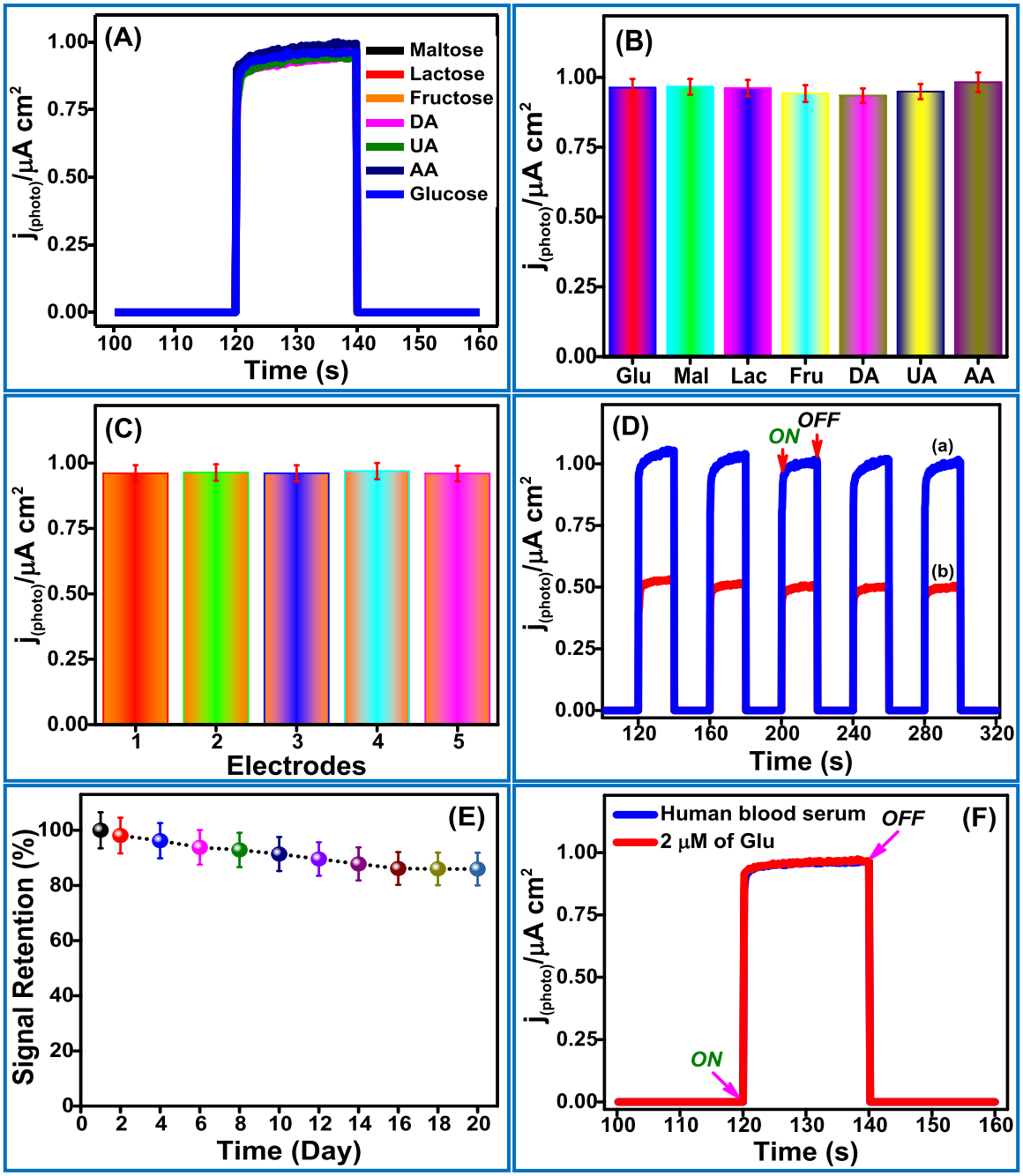

Fig. 5. (A, B) Effect of interferences on the response photocurrents. Experiments were performed in 0.1 M PBS (pH 7.0) containing 2 μM of Glu with maltose, lactose, fructose, DA, UA and AA with light ON. **(C)** Reproducibility on five parallel prepared GODx/NDC-TiO_2NPs/ITO. **D)** Stability under light ON/OFF ((a) presence and (b) absence of 2 μM of glucose) and **(E)** Durability test (over 20 days) of the GODx/NDC-TiO_2NPs/ITO biosensor in the in 0.1 M pH 7.0 PBS. **(F)** The real Glu detection in human blood serum sample.

$$\Delta j_{(photo)} = j_{total} - j_{blank} \quad (1)$$

In Fig. 4(D), it is noted that the GODx/NDC-TiO_2NPs/ITO biosensor provides a perfect linear relationship between [Glu] *versus* $\Delta j_{(photo)}$, with a lower detection limit (LOD) of 13 nM (S/N = 3), high sensitivity (215 nA μM^{-1} cm^{-2}), and a wide linear range from 50 nM to 10 μM (R^2 = 0.9994) under light ON. Also, the analytical performance of our PEC Glu compared with various other Glu sensing materials and tabulated in Table 1. GODx/NDC-TiO_2NPs/ITO biosensor shows enhanced performance in term of ultra-low LOD, linear range and sensitivity when compared to other Glu sensing materials. The ultra-low LOD value for GODx/NDC-TiO_2NPs/ITO biosensor may be ascribed to good electron and hole energy separation and the targeted recognition between the GODx and the Glu. Moreover, the highly conductive NDC provides the greatest improvement in sensitivity of PEC Glu biosensor and leads to the applied bias potential required for driving PEC Glu oxidation to shift towards very low potential (0.4 V *vs.* Ag/AgCl). The results confirmed that the proposed PEC Glu biosensor based on GODx/NDC-TiO_2NPs/ITO has a promising application in the ultrasensing of Glu.

3.5. Interfering effect, reproducibility, stability, and durability

The impact of highly possible coexisting and common molecular interfering species (such as maltose (Mal), lactose (Lac), fructose (Fru), dopamine (DA), uric acid (UA) and ascorbic acid (AA)), which may

affect the PEC Glu sensor response of GODx/NDC-TiO_2NPs/ITO biosensor was investigated. To reveal the selectivity of GODx/NDC-TiO_2NPs/ITO biosensor, PEC experiments were carried out under the same conditions for PEC Glu detection, additionally, the 6 μM of interfering species was added individually to the analyte solution (Fig. 5A). The change of $j_{(photo)}$ after the introduction of interfering species was measured using $j_{(photo)}$-t plots. As shown in Fig. 5A and B, no obvious responses in the PEC detection of Glu were founded after the addition of molecular interfering species, which may be due to the contribution of the surface immobilized GODx on NDC-TiO_2NPs/ITO. This confirmed that the fabricated PEC biosensor based on GODx/NDC-TiO_2NPs/ITO had excellent specific selectivity towards Glu biosensor. To investigate the biosensor fabrication reproducibility, a 2 μM of Glu solution was measured by five GODx/NDC-TiO_2NPs/ITO biosensors using the same fabrication method (Fig. 5C). The fabricated biosensors displayed excellent reproducibility with a relative standard deviation (RSD) value of 3.1%.

Furthermore, the stability of GODx/NDC-TiO_2NPs/ITO biosensor was characterized by $j_{(photo)}$-t responses in both absence and presence of 2 μM of Glu solution when the light ON/OFF repeatedly five cycles in 0.1 M PBS (pH 7.0) (Fig. 5D). When the light was ON, the response of $j_{(photo)}$ rise immediately and reached stable within a few seconds and even after five cycles the GODx/NDC-TiO_2NPs/ITO biosensor shows 98.8% of its initial $j_{(photo)}$ value. In addition, the long-term durability, 2 μM of Glu solution was monitored three times per day. Fig. 5(E) shows the $j_{(photo)}$ response of GODx/NDC-TiO_2NPs/ITO is more stable and retained ~ 86% of its original $j_{(photo)}$ even after 20 days of storage. These results indicate that the GODx/NDC-TiO_2NPs/ITO biosensor reveals an excellent selection, reproducibility, stability, and durability for Glu biosensor, and it might be a capable candidate to monitor real-time Glu.

3.6. Real sample analysis

In addition, the practical application of fabricated PEC Glu sensor was further carried out in human blood serum samples without any pretreatment apart from a dilution step with 0.1 M PBS solution. Fig. 5(F) clearly, illustrate that the $j_{(photo)}$ response to human blood serum sample is well correlated with [Glu] (2 μM) on the GODx/NDC-TiO2NPs/ITO biosensor. Furthermore, the human blood serum used for recovery analyses were pre-tested by commercially available glucometer (CareCens™ N, GM5051A, I-SENS, Inc., Korea). The [Glu] in a diluted human blood serum was determined as 4.22 ± 0.05 μM which is acceptable by comparison with the commercial glucometer value of 4.26 ± 0.032 μM. Different [Glu] were added into diluted human blood serum and evaluated the accuracy of recovery tests from five repeated measurements. The test results, as listed in Table S1, indicated that our GODx/NDC-TiO_2NPs/ITO biosensor has adequate recoveries between 99.02% and 100.17% with RSD 3.31%. This suggesting that our proposed PEC Glu biosensor can be utilized for determination of Glu in practical human blood serum.

4. Conclusion

In summary, we have successfully developed an ultrasensitive photoelectrochemical glucose biosensor, based on nitrogen-doped bio-based carbon (NDC) wrapped TiO_2 NPs (NDC-TiO_2 NPs) synthesized by a new green chemical route and subsequently functionalized with glucose oxidase (GODx/NDC-TiO_2NPs/ITO) for the first time. The electrochemical and photoelectrochemical results reveal that the remarkably improved photoelectrochemical biosensor activity for the developed GODx/NDC-TiO_2NPs/ITO biosensor is attributed to a synergistic effect between bio-derived N and C atoms in NDC, which does not only enhance high conductivity, but also significantly facilitates the charge separation and good charge carrier shuttling process between the FED redox center of GODx and the biosensor surface. As a proof-of-concept, the GODx/NDC-TiO_2NPs/ITO based PEC glucose biosensor exhibit the low detection range of 13 nM and a wide linear range (0.05–10 μM) under optimized PEC experimental conditions. The photoelectrochemical glucose detection in real human blood serum was also revealed with good recoveries (99.02–100.17% and RSD 3.31%). Thus, we predict that the given PEC biosensor fabricated from the sustainable process is a promising platform for extending the other photoelectrochemical biosensors through careful selection of an enzyme and photo-electroactive materials. Also, we believe that the sustainable strategies for heteroatom co-doping could improve with other semiconductor photoelectrodes and their photoelectrochemical applications.

Acknowledgments

This research was partially supported by the Nano Material Technology Development Program of the Korean National Research Foundation (NRF) funded by the Korean Ministry of Education, Science, and Technology (2012M3A7B4049675) and the Priority Research Centers Program (2014R1A6A1031189). This work was supported by the National Research Foundation (NRF) of Korea grant funded by the Ministry of Science, Information and Communications Technology (MSIT) of Korea government (2017R1C1B5076345). N. Muthuchamy and K. H. Park were supported by Basic Science Research Program through the National Research Foundation of Korea (NRF) funded by the Ministry of Science, ICT & Future Planning (2017R1A4A1015533 and 2017R1D1A1B03036303).

Electronic supplementary information (ESI) available

Synthesis procedure, Raman spectrum and ATR-FTIR spectrum of the synthesized NDC-TiO_2NPs. FESEM images of the synthesized bare TiO_2 NPs. The active surface area calculation, chronoamperometric response of GODx/NDC-TiO_2NPs/ITO electrode in the absence of light, effect of catalyst loading, GODx loading, supporting electrolyte pH value and applied potential on PEC responses. Table S1. Concentration of Glu in real (Human serum) samples measured by the commercial glucometer and by the proposed PEC biosensor.

Appendix A. Supporting information

Supplementary data associated with this article can be found in the online version at doi:10.1016/j.bios.2018.10.049

References

Atchudan, R., Edison, T.N.J.I., Aseer, K.R., Perumal, S., Karthik, N., Lee, Y.R., 2018a. Biosens. Bioelectron. 99, 303–311.
Atchudan, R., Edison, T.N.J.I., Perumal, S., Vinodh, R., Lee, Y.R., 2018b. J. Alloy. Compd. 766, 12–24.
Atchudan, R., Edison, T.N.J.I., Aseer, K.R., Perumal, S., Lee, Y.R., 2018c. Colloids Surf. B 169, 321–328.
Atchudan, R., Edison, T.N.J.I., Perumal, S., Karthikeyan, D., Lee, Y.R., 2017. J. Photochem. Photobiol. 333, 92–104.
Başkaya, G., Yıldız, Y., Savk, A., Okyay, T.O., Eriş, S., Sert, H., Şen, F., 2017. Biosens. Bioelectron. 91, 728–733.
Bettazzi, F., Laschi, S., Voccia, D., Gellini, C., Pietraperzia, G., Falciola, L., Pifferi, V., Testolin, A., Ingrosso, C., Placido, T., Comparelli, R., 2018. Electrochim. Acta 276, 389–398.
Campos, B.B., Abellán, C., Zougagh, M., Jimenez-Jimenez, J., Rodríguez-Castellón, E., Esteves da Silva, J.C.G., Algarra, M., Ríos, A., 2015. J. Colloid Interface Sci. 458, 209–216.
Chen, D., Zhang, H., Liu, Y., Li, J., 2013. Energy Environ. Sci. 6 (5), 1362–1387.
Dai, H., Zhang, S., Gong, L., Li, Y., Xu, G., Lin, Y., Hong, Z., 2015. Biosens. Bioelectron. 72, 18–24.
Devadoss, A., Sudhagar, P., Terashima, C., Nakata, K., Fujishima, A., 2015. J. Photochem. Photobiol. C 24, 43–63.
Ding, H., Wei, J.S., Xiong, H.M., 2014. Nanoscale 6 (22), 13817–13823.
Gnanasekaran, L., Hemamalini, R., Ravichandran, K., 2015. J. Saudi Chem. Soc. 19 (5), 589–594.
Gopalan, A.I., Komathi, S., Muthuchamy, N., Lee, K.P., Whitcombe, M.J., Lakshmi, D.,

Sai-Anand, G., 2018. Prog. Polym. Sci. https://doi.org/10.1016/j.progpolymsci.2018.08.001.
Gopalan, A.I., Muthuchamy, N., Lee, K.P., 2017. Biosens. Bioelectron. 89, 352–360.
Guo, Q., Liu, L., Zhang, M., Hou, H., Song, Y., Wang, H., Zhong, B., Wang, L., 2017. Biosens. Bioelectron. 92, 654–660.
Gupta, S., Smith, T., Banaszak, A., Boeckl, J., 2018. MRS Adv. 3 (15–16), 831–847.
Hao, N., Zhang, X., Zhou, Z., Qian, J., Liu, Q., Chen, S., Zhang, Y., Wang, K., 2017. Sens. Actuators B 250, 476–483.
Ibrahim, I., Lim, H.N., Zawawi, R.M., Tajudin, A.A., Ng, Y.H., Guo, H., Huang, N.M., 2018. J. Mater. Chem. B 6, 4551–4568.
Jang, H.D., Kim, S.K., Chang, H., Roh, K.M., Choi, J.W., Huang, J., 2012. Biosens. Bioelectron. 38 (1), 184–188.
Ju, J., Chen, W., 2014. Biosens. Bioelectron. 58, 219–225.
Komathi, S., Gopalan, A.I., Muthuchamy, N., Lee, K.P., 2017. RSC Adv. 7 (25), 15342–15351.
Komathi, S., Muthuchamy, N., Lee, K.P., Gopalan, A.I., 2016. Biosens. Bioelectron. 84, 64–71.
Li, W., Yue, Z., Wang, C., Zhang, W., Liu, G., 2013. RSC Adv. 3 (43), 20662–20665.
Li, H., Kong, W., Liu, J., Liu, N., Huang, H., Liu, Y., Kang, Z., 2015. Carbon 91, 66–75.
Liu, P., Huo, X., Tang, Y., Xu, J., Liu, X., Wong, D.K., 2017a. Anal. Chim. Acta 984, 86–95.
Liu, X., Huo, X., Liu, P., Tang, Y., Xu, J., Liu, X., Zhou, Y., 2017b. Electrochim. Acta 242, 327–336.
Lou, Z., Huang, H., Li, M., Shang, T., Chen, C., 2013. Materials 7 (1), 97–105.
Muthuchamy, N., Atchudan, R., Edison, T.N.J.I., Perumal, S., Lee, Y.R., 2018. J. Electroanal. Chem. 816, 195–204.
Muthuchamy, N., Lee, K.P., Gopalan, A.I., 2017. Biosens. Bioelectron. 89, 390–399.
Nallal, M., Anantha Iyengar, G., Pill-Lee, K., 2017. ACS Appl. Mater. Interfaces 9 (42), 37166–37183.
Niu, W.J., Li, Y., Zhu, R.H., Shan, D., Fan, Y.R., Zhang, X.J., 2015. Sens. Actuators B 218, 229–236.
Santhiago, M., Garcia, P.S., Strauss, M., 2018. Curr. Opin. Green Sustain. Chem. 12, 22–26.
Shang, M., Qi, H., Du, C., Huang, H., Wu, S., Zhang, J., Song, W., 2018. Sens. Actuators B 266, 71–79.
Vashist, S.K., 2012. Anal. Chim. Acta 750, 16–27.
Wang, Y., Bai, L., Wang, Y., Qin, D., Shan, D., Lu, X., 2018. Analyst 143 (7), 1699–1704.
Yang, Z., Xu, M., Liu, Y., He, F., Gao, F., Su, Y., Wei, H., Zhang, Y., 2014. Nanoscale 6, 1890–1895.
Zhang, L., Ruan, Y.F., Liang, Y.Y., Zhao, W.W., Yu, X.D., Xu, J.J., Chen, H.Y., 2018. ACS Appl. Mater. Interfaces 10 (4), 3372–3379.
Zhang, R., Chen, W., 2014. Biosens. Bioelectron. 55, 83–90.
Zhao, W.W., Xu, J.J., Chen, H.Y., 2014. Chem. Rev. 114 (15), 7421–7441.
Zhao, Y., Gong, J., Zhang, X., Kong, R., Qu, F., 2018. Sens. Actuators B 255, 1753–1761.
Zhu, W., Wang, J., Zhang, W., Hu, N., Huang, L., Wang, R., Suo, Y., Wang, J., 2018. J. Mater. Chem. B 6 (5), 718–724.